CONF-9610205--3
ANL/TD/CP--91547

IRRADIATION BEHAVIOR OF URANIUM OXIDE - ALUMINUM DISPERSION FUEL*

Gerard L. Hofman, Jeffrey Rest and James L. Snelgrove

Argonne National Laboratory
Argonne, IL 60439-4841

To be presented at the
1996 International Meeting on Reduced Enrichment
for Research and Test Reactors

October 7-10, 1996
Seoul, Korea

*Work supported by hte U.S. Department of Energy
Office of Nonproliferation and National Security
under Conntract No. W-31-109-38-ENG

DISCLAIMER

IRRADIATION BEHAVIOR OF URANIUM OXIDE - ALUMINUM DISPERSION FUEL

Gerard L. Hofman, Jeffrey Rest and James L. Snelgrove
Argonne National Laboratory
Argonne, IL

ABSTRACT

An oxide version of the DART code has been generated in order to assess the irradiation behavior of UO_2-Al dispersion fuel. The aluminum-fuel interaction models were developed based on U_3O_8-Al irradiation data. Deformation of the fuel element occurs due to fuel particle swelling driven by both solid and gaseous fission products, as well as a consequence of the interaction between the fuel particles and the aluminum matrix. The calculations show, that with the assumption that the correlations derived from U_3O_8 are valid for UO_2, the LEU UO_2-Al with a 42% fuel volume loading (4 gm/cc) irradiated at fuel temperatures greater than 413 K should undergo breakaway swelling at core burnups greater than about $1.12X10^{27}$ fissions m^{-3} (~63 % ^{235}U burnup).

INTRODUCTION

Previous postirradiation data from U_3O_8-Al dispersion fuel miniplates[1, 2, 3] have been reanalyzed. These test plates were manufactured by Oak Ridge National Laboratory, CNEA and NUKEM and were irradiated in ORR as part of the RERTR program. The purpose of this reanalysis was to develop a computational irradiation behavior model for uranium oxide-aluminum dispersion fuel that can be used to predict the irradiation behavior of UO_2-Al (LEU) dispersion fuel to be fabricated and tested as part of a US-Russian cooperative RERTR program.

The ANL DART code[4] was used in this work. This code was originally developed for uranium silicide-aluminum dispersion fuel. To adapt the code for uranium oxide fuel, published information on the behavior of U-oxide in aluminum was utilized in modifying various models in the code.

POSTIRRADIATION MICROSTRUCTURE

The basic microstructural features revealed by postirradiation metallography of 80% enriched, 32 wt. % UO_2 (80% burnup), and 45% enriched U_3O_8 (47% burnup) dispersed in aluminum are shown in Fig. 1. Both oxides appear to be rather similar, having a globular shaped phase at the center of the fuel particles, surrounded by a smooth dark phase and a multi-phase interaction product at the aluminum matrix interface. Previous work at ORNL[5] with an election-

microprobe clearly showed the extent of aluminum-oxide interaction; only the globular phase remains free of aluminum (see Fig. 2). This is presumably unreacted fuel. The two other phases have clearly different uranium and aluminum concentrations. A more recent study with a scanning electron microscope and an Auger spectroscope[6] has yielded additional information, allowing a more precise characterization of this widely used dispersion fuel. As shown in Fig. 3, the phase identified as "2" in Martin's work actually consists of two phases. These are, judging from electron back-scatter images, most likely the UAl_4 and Al_2O_3 reaction products. The other aluminum-containing phase ("3" in Martin's work) has a U/O ratio near that of U_3O_8. This phase is the original U_3O_8 into which substantial aluminum has diffused. The globular phase that contains no aluminum has a U/O ratio equal to that of U_4O_9 (see Table I). The microstructure of this reacted U_3O_8, combined with the information learned in previous work, can help explain the swelling behavior of this dispersion fuel. The globular phase is presumably U_4O_9, a cubic phase similar to UO_2. The granular appearance of the fracture surface shown in Fig. 4 suggests that the grain refinement previously observed in UO_2 has occurred here and that the swelling behavior of this phase is similar to that of UO_2[7]. Phase "3", U_3O_8 containing aluminum, has a smooth-glassy fracture surface and contains some relatively large gas bubbles. U_3O_8 was found to become amorphous during irradiation[8]; this may account for its appearance and the evidently high diffusivity of aluminum at these low temperatures.

Table I. Results of Auger Microprobe Analysis on Irradiated U_3O_8 Al Dispersion Fuel.

Phase	U	O	Al (at.%)	O/M[a]
3	23	62	15	2.7 (U_3O_8)
4	31	69	0	2.2 (U_4O_9)

[a] Oxygen-to-metal ratio.

More important to the overall swelling behavior is the UAl_4-Al_2O_3 mixed reaction phase. We may assume that Al_2O_3 is amorphous and very plastic due to recoil damage from the finely dispersed UAl_4, giving rise to the relatively large bubbles observed to be formed in this phase (see Fig. 5). So long as the reacted fuel particles remain largely isolated, as in a moderately loaded dispersion such as shown in Fig. 1, swelling will be very modest and predictable to a very high burnup. However, in highly loaded dispersions, where most of the matrix aluminum may be consumed by the reaction, there is a definite limit to fission gas retention of the UAl_4-Al_2O_3 phase, as is evident in the micrograph of LEU fuel shown in Fig. 5. Continued fissioning results in rapid swelling due to very large interconnected bubbles in the reaction phases and, eventually in failure of the fuel plate. The limiting conditions in terms of loading and burnup capability of the fuel are shown schematically in Fig. 6. Here we have used fission density in the meat as opposed to fission density in the fuel particle as the variable since the original fuel particle has been lost through reaction.

These reactions result in a net decrease in volume, and therefore represent a negative core swelling component. Published data from HFIR[12], MTR [13], and SRL[14] were used to develop a correlation for the rate of reaction between U_3O_8 and aluminum. The correlation, expressed in terms of the width, y, of the interaction zone at the periphery of an assumed average spherical fuel particle is shown in Fig. 8 and is of an Arrhenius type;

$$y^2/t = k \exp\left(-\frac{Q}{RT}\right) \tag{4}$$

where t in the irradiation times in seconds
y the reactor depth is μm
k the reaction rate constant
Q the activation energy in Kcal $mole^{-1}$

This correlation predicts the U_3O_8-Al reaction, measured by quantitative metallography, of the ORR miniplates that are used in this analysis (see Figs. 8 and 9).

The DART mechanical analysis addresses the mechanical behavior of dispersion fuel plates, tubes, and fuel rods. The model examines a system of spherical fuel particles surrounded by a large spherical shell of matrix material bonded to an outer shell of aluminum cladding. This approach treats the inner sphere as an elastically deforming body and the spherical shell as perfectly plastic. The DART swelling models provide the driving force for mechanical deformation. The model is derived directly from the equations of equilibrium, compatibility, strain displacement, and the constitutive equations (stress-strain relationships) coupled with the assumption of incompressibility of plastic strains. The boundary conditions assume finite radial stresses at the center of the inner sphere, no discontinuity in the radial stress at the fuel/matrix interface, and no pressure on the outer surface of the spherical shell. It is also assumed that thermal expansion and swelling are not functions of radial position and that the outer radius of the spherical shell approaches infinity. This approach to thermal and swelling strains is based on calculations that indicate the temperature changes across a fuel plate or rod are small.

No change in yield stress with fluence is considered. Evaluation of available data indicates that the change in yield stress due to fluence is negligible. Inclusion of this phenomenon will slightly reduce deformation estimates. In addition, the effects of irradiation-enhanced creep and irradiation hardening are not considered. Consideration of these phenomena would require time-dependent deformation analysis, which would add significantly to the complexity and execution efficiency of the DART code. The effects of irradiation-enhanced creep and hardening are accounted for by the inclusion of a phenomenological factor that multiplies the aluminum yield strength. The value of this factor depends on the geometry of the element, i.e. plate or rod.

The model consists of the stress analysis of a hard sphere of radius a, assumed to behave elastically, surrounded by a spherical shell with outer radius b of a softer material that is assumed to behave in a perfectly plastic manner $(b>>a)$. This plastic behavior is assumed to extend out to a plastic radius r_c such that $a<r_c<b$. This procedure yields an equation for the interfacial pressure (radial stress) at the fuel/matrix interface in terms of fuel particle swelling and plastic

deformation in the matrix (i.e., as the interfacial pressure increases, plastic flow is induced in the matrix out to some radius beyond which only elastic deformation occurs). Based on the results of a general solution to the problem, an approximation is introduced that avoids the simultaneous solution of the interfacial pressure and the radius of plastic deformation. For positive interface pressure P_i,

$$P_i = 2\left[\frac{1}{3} + ln\left(\frac{r_c}{a}\right)\right] S_y \tag{5}$$

where S_y is the yield stress determined from the von Mises criterion for plastic flow. The results of the general solution indicate that r_c increases rapidly to include most of the matrix aluminum. Thus, it appears reasonable to make the approximation that the fuel volume fraction is give by

$$\frac{V_o^f + \Delta V^f}{V_o^c} = \frac{4/3\pi\ a^3}{4/3\pi\ r_c^3} = \left(\frac{a}{r_c}\right)^3, \tag{6}$$

where $\frac{V_o^f}{V_o^c}$ is the as-fabricated fuel volume fraction in the core and $\frac{\Delta V^f}{V_o^c}$ is the increase in fuel volume fraction due to processes such as as-fabricated pore closure and fuel particle swelling. Thus from Eqs. 5 and 6,

$$P_h = P_i = \frac{2}{3}\left[1 - ln\left(\frac{V_o^f + \Delta V_f}{V_o^e}\right)\right]\beta_{Al}\ S_y, \tag{7}$$

where P_i has been identified with the hydrostatic stress within the fuel particle P_h, and β_{Al} is a phenomenological factor (discussed above) that has been introduced to account for the effects of irradiation (e.g., irradiation-enhanced creep and hardening). The value of β_{Al} used for describing fuel plates and tubes is 0.13.

The growth of fission gas bubbles depends on the hydrostatic pressure P_h in the fuel adjacent to the bubble surface. Equation 7 relates P_h to the overall fuel volume fraction and the aluminum yield stress and therefore provides an estimate of the average hydrostatic stress within the fuel particle. As seen in the above sections, a gradient in fuel composition will, in general, exist across fuel particle. This phase gradient will give rise to the gradient in swelling, and thus a gradient in stress. To realistically calculate the fission gas bubble size distributions and hence fuel swelling, a mechanism for evaluating the stress gradient within the fuel particle must be introduced.

DART employs a radial nodalization scheme to characterize temperature, stress, swelling, and phase gradients. As discussed above a phenomenological factor has been introduced in the elastic/perfectly plastic analysis of fuel particle deformation within an aluminum matrix to account for the effects of irradiation (e.g., irradiation-enhanced creep and hardening) without

resorting to a much more complicated time-dependent deformation analysis. The fuel-aluminum reaction moves from the fuel particle surface inward. When the reaction front has crossed a fuel node, that node is considered transformed to the reaction-product phase, and the nodal volume change due to the reaction is implemented, as well as the volume change in the matrix due to the loss of aluminum. The total core swelling (TCS) is given by

$$TCS = FPS + RPS + AFP, \tag{8}$$

where FPS = fission product swelling, RPS = reaction product swelling, and AFP = as-fabricated porosity. The swelling fuel particles cause yielding of the matrix aluminum and cladding deformation. During the initial phase of the irradiation when both the fuel volume fraction and the volume fraction of reaction product is considerably less than the volume fraction of aluminum matrix, the swelling rate primarily depends on the plastic yielding of the aluminum matrix and cladding. As amount of reaction product increases, the swelling rate will depend more on the "yielding" of the amorphous reaction product than on the plastic yielding of the remaining aluminum matrix. It is assumed in the analysis that when the aluminum volume fraction reaches 10%, the effect of the yielding of the amorphous reaction product becomes important. At this point, the effective yield strength $\beta_{Al} S_y$ of aluminum in Eq. 7 is replaced with the effective yield strength of the two-phase mixture, i.e.,

$$\beta_{Rp} = \beta_{al} / (1 - VAM/0.01) + 1],$$

where VAM is the aluminum volume fraction. Thus, from Eq. 9, when the matrix aluminum has completely disappeared, the effective yield strength is reduced by a factor of 3.5.

CALCULATIONS

A. U_3O_8-Al

Figures 10-12 show the results of DART calculations at 100°C for fission-product swelling, reaction swelling, total swelling, and as-fabricated porosity as a function of the core fission density compared with data from LEU and MEU U_3O_8-Al irradiations of plates with with fuel loadings of 44% (Fig. 12), 39% (Fig. 11), and 35% (Fig. 10), respectively. The total swelling during the early phase of irradiation is negative due to the sintering of the as-fabricated porosity and core shrinkage due to the reaction between the U_3O_8 and the matrix aluminum. Subsequent to the sintering of the as-fabricated porosity, the total swelling increases due to fission product swelling. Recrystalization of the fuel leads to enhanced swelling rates (at about 1 x 10^{27} fissions m^{-3} in Figs. 10-12). As the irradiation proceeds and the fuel continues to react with the matrix aluminum, the fuel volume fraction increases while the aluminum volume fraction decreases (see Fig. 13). Thus, the morphology of the core evolves from U_3O_8 fuel particles in an aluminum matrix to UO_2 (or U_4O_9) particles surrounded by increasing amounts of UAl_x and Al_2O_3, reaction products, and decreasing amounts of aluminum matrix. Al_2O_3 is amorphous, and the composite reaction product is presumably much softer and more ductile than the matrix aluminum. In addition, fission gas bubbles grow at an enhanced rate in the irradiated amorphous reaction product. This is analogous to bubble behavior in irradiated U_3Si.

The transition from swelling fuel particles surrounded by a yielding aluminum matrix to fuel particles surrounded by a considerably softer reaction product matrix is described by the effective yield stress formulation given in Eqs. 7-9; that is, when the aluminum volume fraction reaches 10% (see Fig. 13), the assumption is made that the presence of the reaction product starts affecting the effective yield stress. The effective yield stress of the reaction product is assumed to be a factor of 3.5 times softer than that for the matrix aluminum.

This transition occurs in the 44% case (Fig. 12) at about 1.5 x 10^{27} fissions m^{-3} where the swelling rate increases due to the presence of fission gas bubbles in the "weaker" amorphous reaction product. As can be seen from Fig. 12, this formulation provides a plausible interpretation of the data. The calculations shown in Figs. 11 and 13 for the 39% case are also in agreement with the observations. The 39% case reaches 10% aluminum volume fraction at about 2.25 x 10^{27} fissions m^{-3} (Fig. 13) and failure of the plate (200% swelling) occurs by 2.5 x 10^{27} fissions m^{-3}. In contrast to the 39 and 44% fuel loading cases discussed above, the 35% case remains stable throughout the irradiation. The calculations for this irradiation, shown in Fig. 10, predict that the irradiation is stable because the aluminum volume fraction never drops below 10%.

The model predicts a much more rapid failure of the 39 vol.% plate than of the 44 vol.% plate, as seen by comparing Figs 11 and 12. The explanation is as follows. Since a much longer irradiation time is required to reduce the aluminum volume fraction to 10% in the 39 vol.% plate than in the 44 vol.% plate, a much larger amount of fission gas is available to drive the swelling, resulting in a more rapid expansion of the gas bubbles.

B. UO_2-Al

To calculate the swelling in tubular MR elements, it is assumed that the models derived for U_3O_8 also apply to UO_2 and machined analysis shows that the relatively large diameter thin wall fuel tubes behave as fuel plates. It is further assumed that the average UO_2 particle size is 80 μm, and the fuel loading at 4 g LEU cm^{-3} is 42 vol. %. Because core temperature and as-fabricated porosity are not known, two values for each of these parameters were chosen, i.e., 100°C and 140°C, and 5 and 10 vol.%, respectively.

The results shown in Figs. 14 and 15 indicate that for the 100°C cases, the core swelling is moderate and no pillowing of the tubes is anticipated below ~86% of the ^{235}U. Fig. 16 shows the predicted change in core constituent volume fractions as the irradiation proceeds for the case with 5% as-fabricated porosity.

In the case of 140°C, shown in Figs. 17 and 18, the core swelling is much larger, ~30% at full burnup. This is due to the fact that all matrix aluminum is consumed early in the irradiation (see Fig. 19), and fission gas bubble growth in the reaction product

occurs over a relatively long irradiation interval. Based on the U_3O_8 experience (see Figs. 11 and 12), swelling values of ~20% in a fully reacted core are likely to be either at the threshold of or already in the pillowing stage.

CONCLUSIONS

The DART aluminum-fuel interaction models were developed based on U_3O_8-Al irradiation data. An initial evaluation of UO_2-Al data indicates that the aluminum matrix/fuel reaction in UO_2 is similar to that in U_3O_8-Al. Excessive deformation of the tubular fuel element occurs when the aluminum volume fraction decreases to about 10%. At this point, fuel particle swelling driven by gaseous fission products is restrained by a "weak" amorphous reaction product and the relatively "weak" tube wall. The combination of an aluminum volume feraction < 10% and meat swelling > 20% provides a breakaway swelling criterion based on the analysis of the U_3O_8-Al irradiation data. The DART calculations predict that LEU UO_2-Al with a 42% fuel volume loading (4 gm/cc) and 5% initial porosity irradiated at a fuel temperaturee of 413 K will undergo breakaway swelling at a core burnup of about 1.12×10^{27} fission m^{-3} (~63% ^{235}U burnup). On the other hand, if the irradiation temperature is lowered to 373 K, breakaway swelling is not predicted to occur until 1.47×10^{27} fissions m^{-3} (~86% ^{235}U burnup).

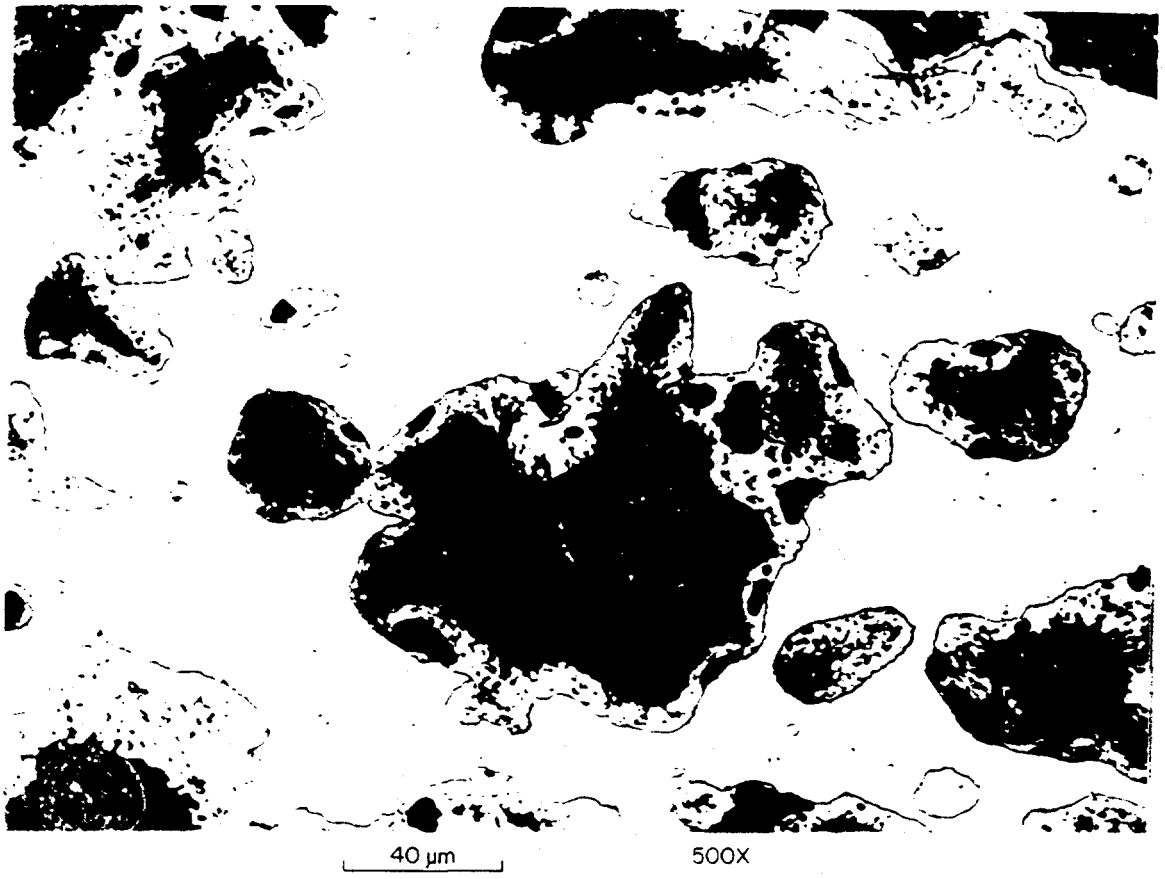

A. 80% Burnup

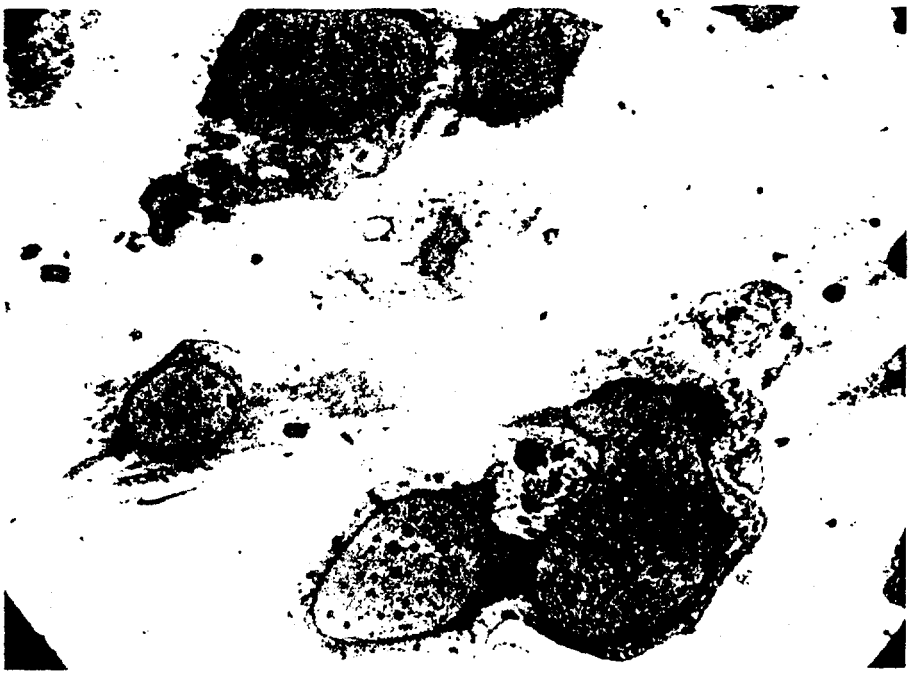

As Polished 500X

B. 47% U^{235} Burnup[B]

Fig. 1. Microstructure of 80% Enriched UO_2, 32 wt. % UO_2 [B] and 45% Enriched U_3O_8 [A] Dispersed in Al

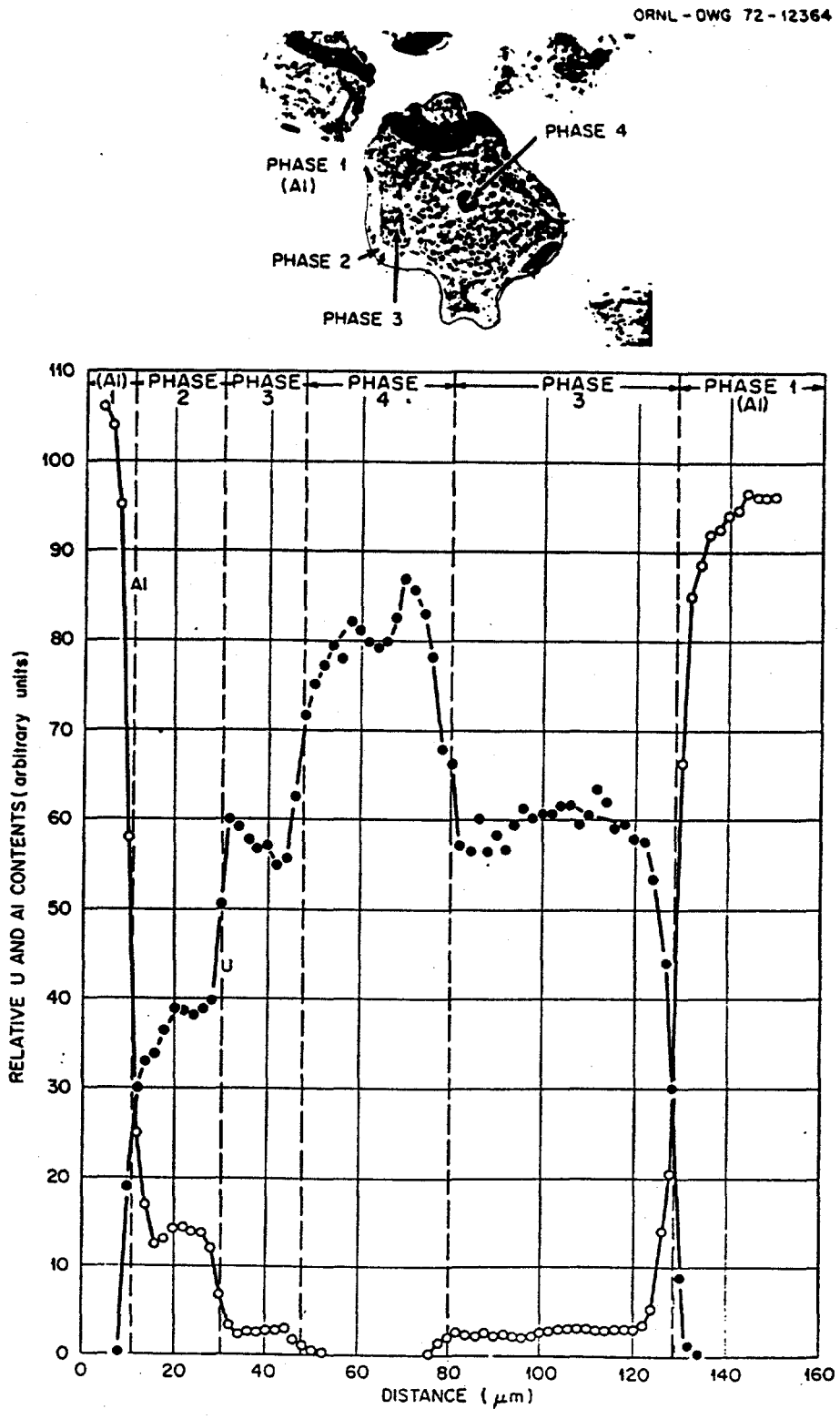

Fig. 2. Relative Uranium and Aluminum Distribution Across a Typical Fuel Particle of an Irradiated U_3O_8 Fuel Dispersion.

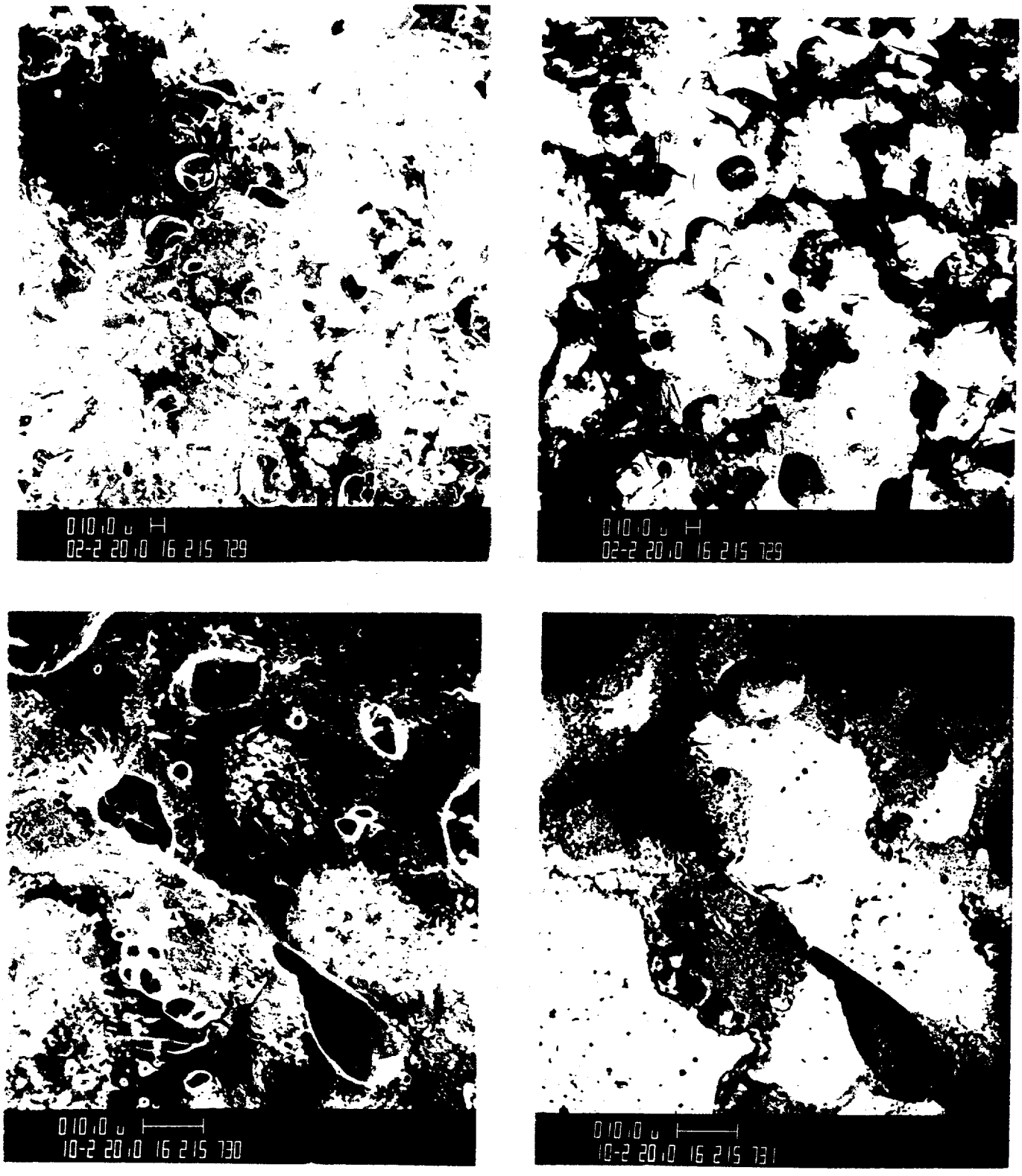

Fig. 3. Various Phases and Bubble Morphology in U_3O_8-Al Plate Orr Irradiation.

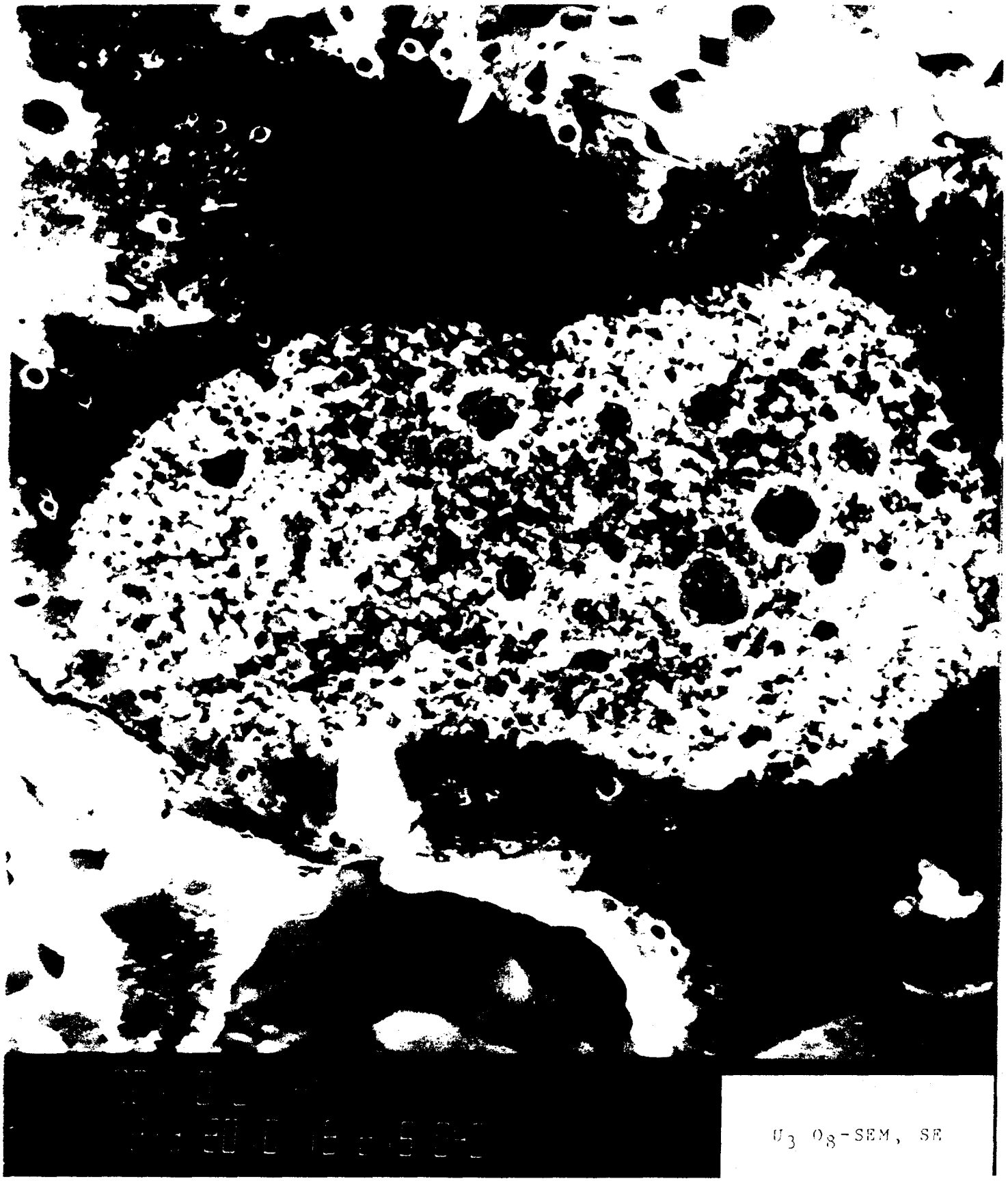

Fig. 4. Center (unreacted) Part of Uranium Oxide Particle Showing Grain Refinement

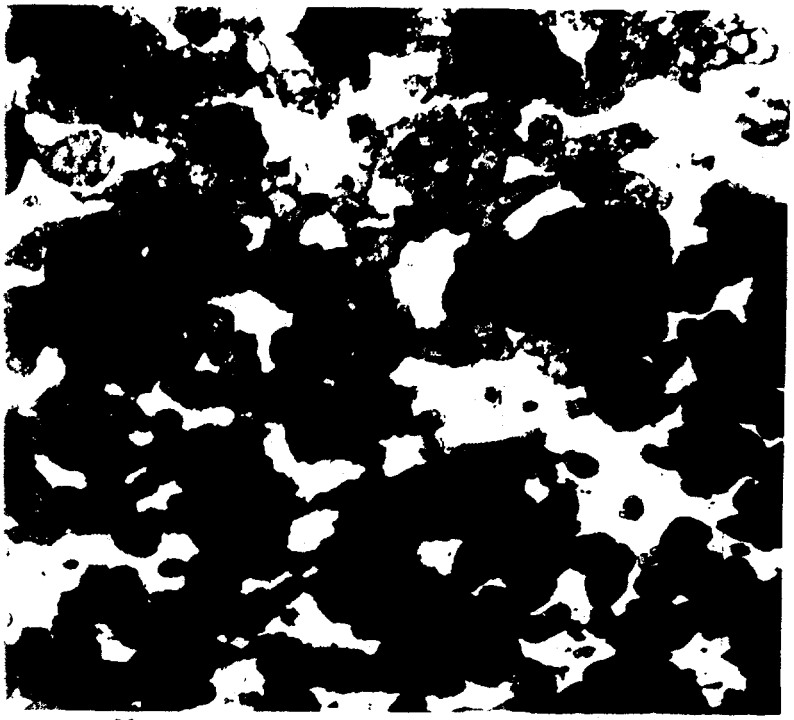

-54-2 Shows Fuel Particles, Reaction Zone, and Unreacted
-1, 70 wt % U_3O_8, 20% Enriched).

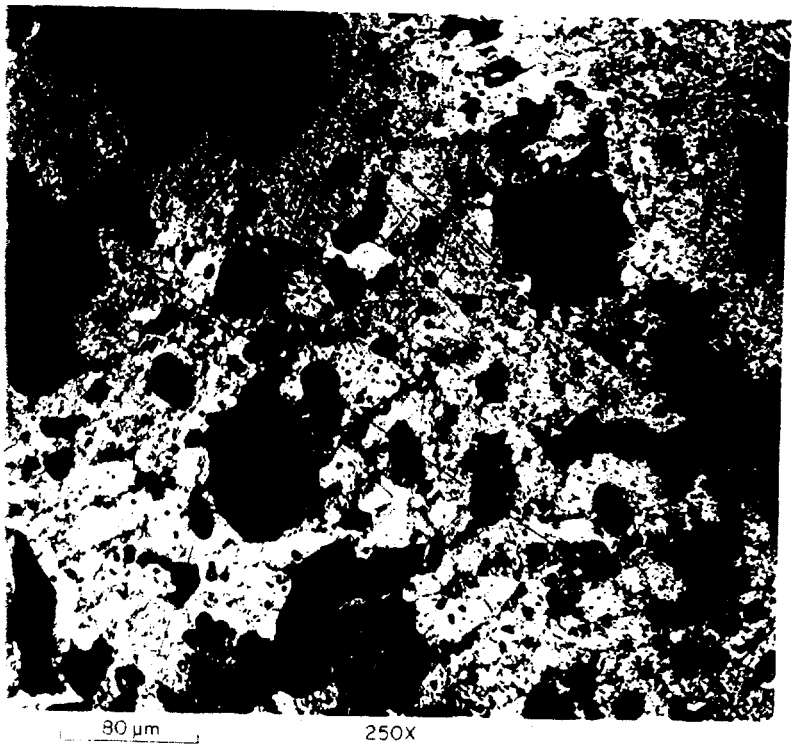

-1-1 Shows Melt Completely Reacted with Shell Islands
-1, 75 wt % U_3O_8, 15% Enriched).

Fig. 5.

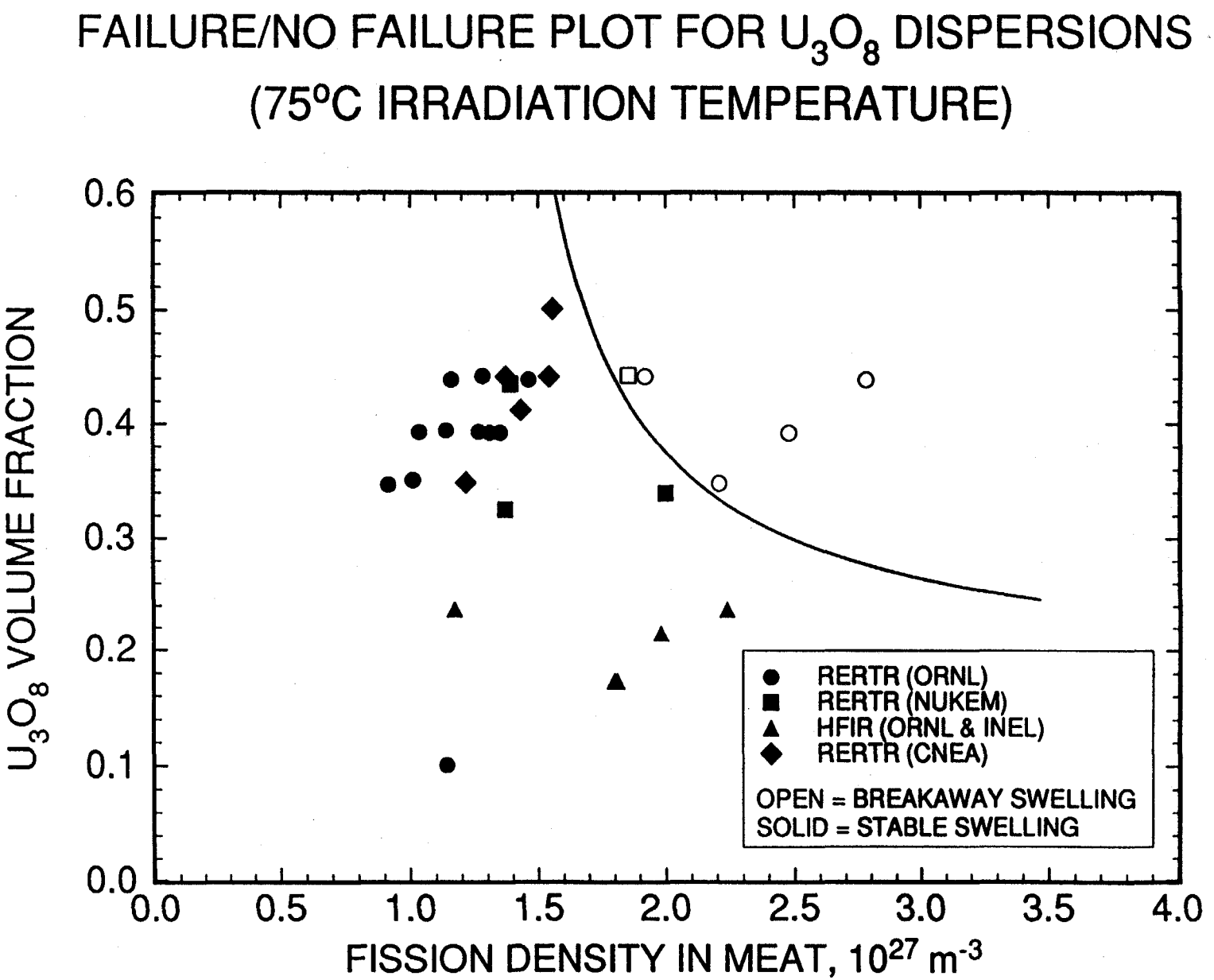
FAILURE/NO FAILURE PLOT FOR U_3O_8 DISPERSIONS
(75°C IRRADIATION TEMPERATURE)
U_3O_8 VOLUME FRACTION
0.0
0.1
0.2
0.3
0.4
0.5
0.6
0.0
0.5
1.0
1.5
2.0
2.5
3.0
3.5
4.0
FISSION DENSITY IN MEAT, 10^{27} m^{-3}
RERTR (ORNL)
RERTR (NUKEM)
HFIR (ORNL & INEL)
RERTR (CNEA)
OPEN = BREAKAWAY SWELLING
SOLID = STABLE SWELLING

Fig. 6.

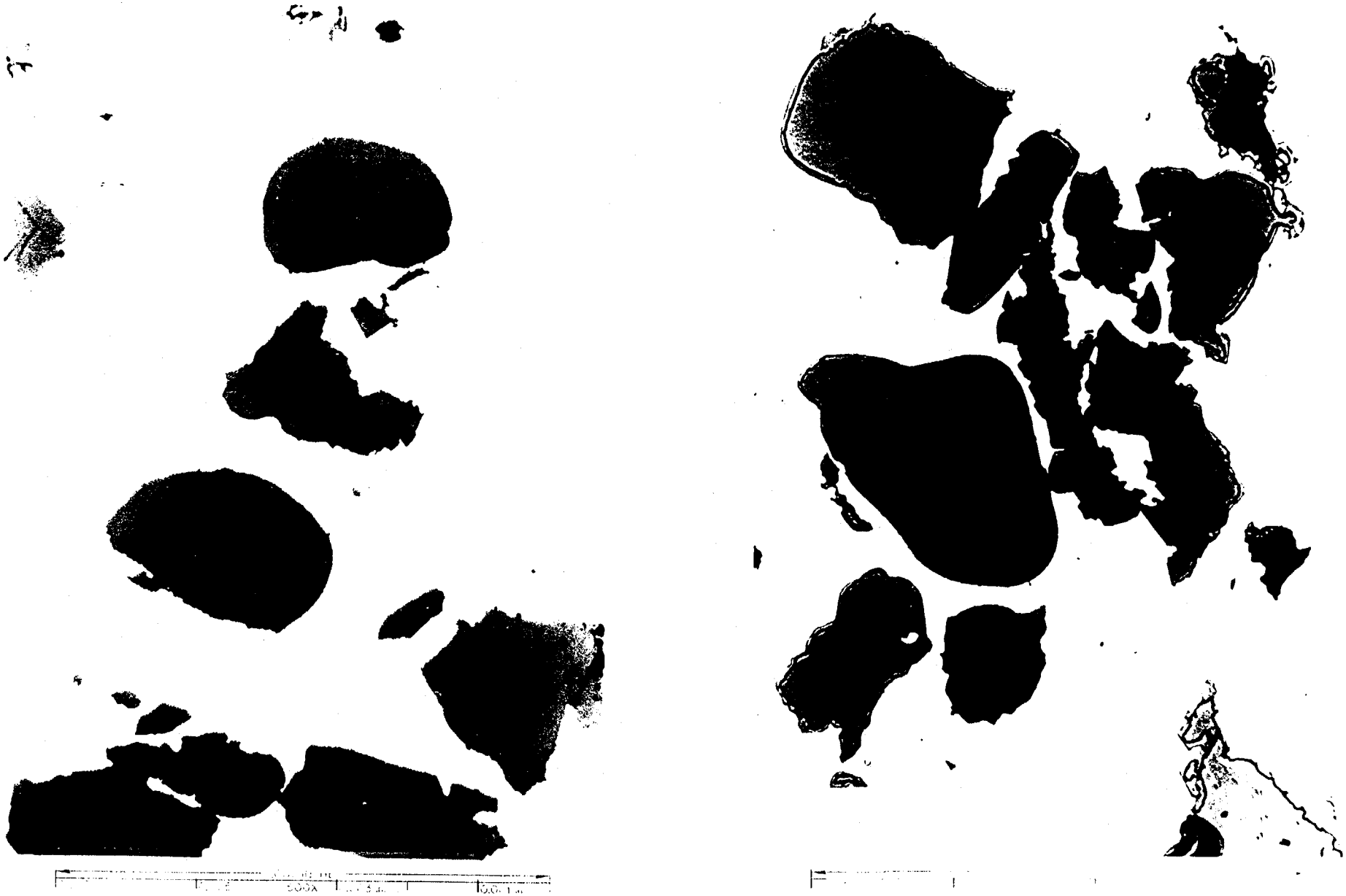

Fig. 7. Depleted U_3O_8

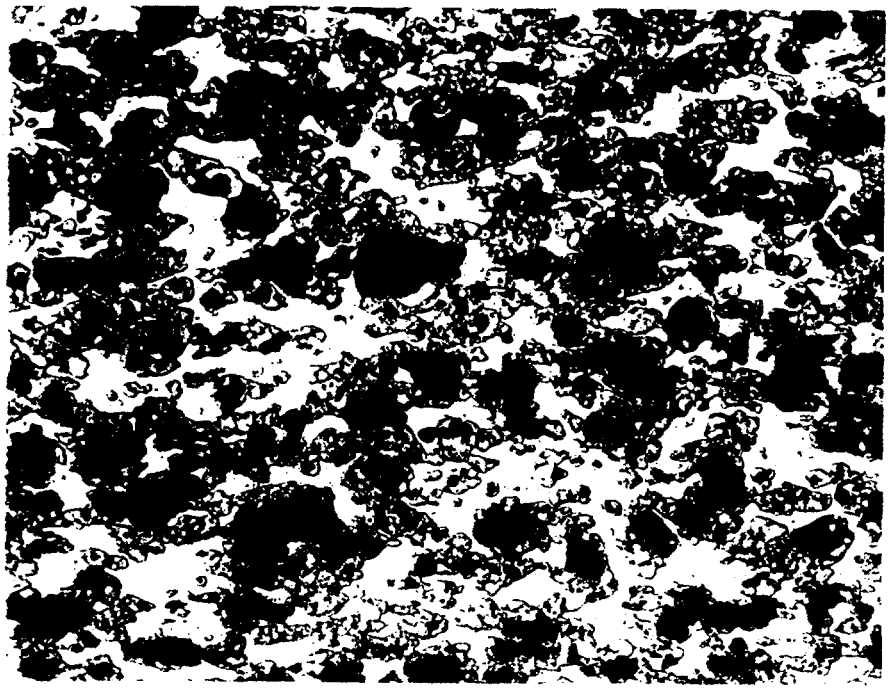

As polished @ 100K

	As Fabricated, Vol.%	FD^{Core}, 1.14 x 10^{27} m^{-3}, Vol.%
Porosity	8	12
Aluminum	53	23
Fuel	39	26
Reaction Phase	0	39

Fig. 9. Results of Qualitative Image Analysis on Miniplate 054-2 with Original 70 wt.% U_3O_3, after Irradiation in ORR to a Core Fission Density of 1.15 10^{27} m^{-3}.

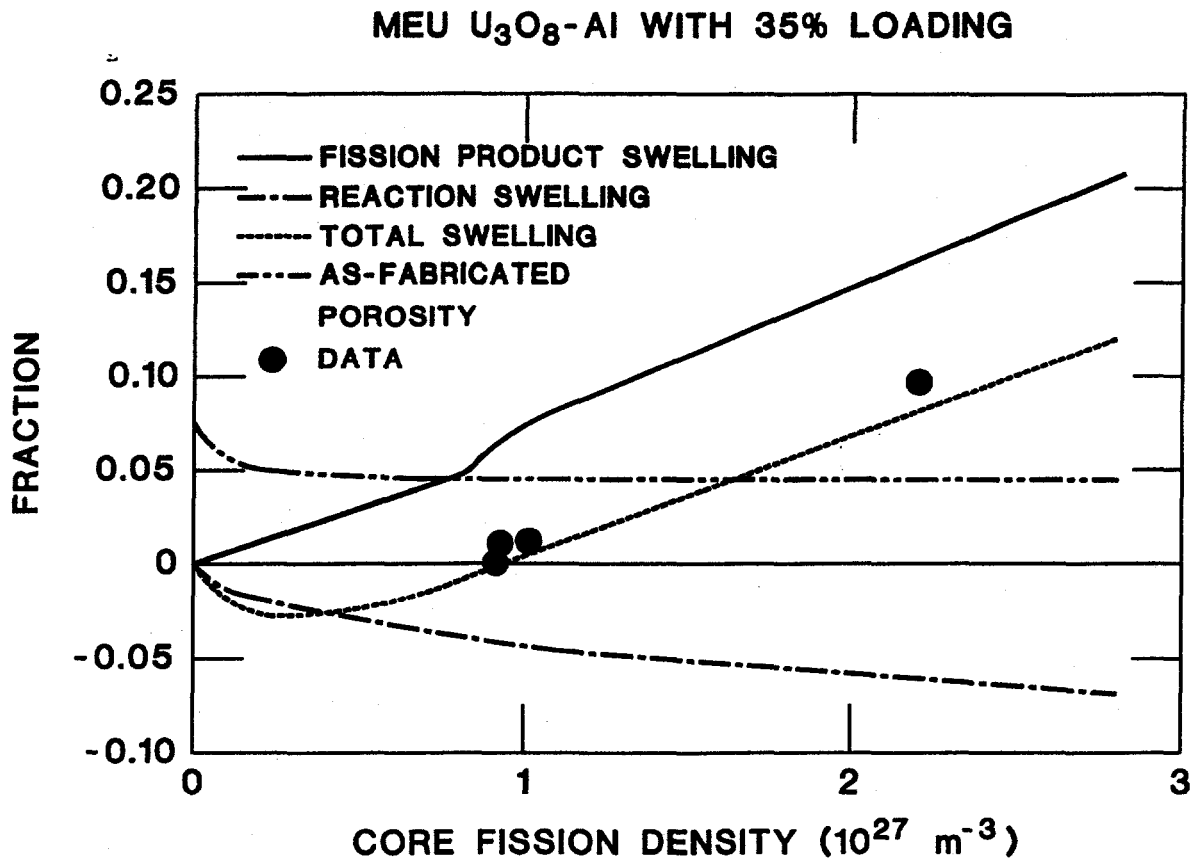

Fig. 10. DART Calculation for MEU U_3O_8-Al Plate with 35 vol.% Loading and LEU and MEU Miniplate Core Swelling Data

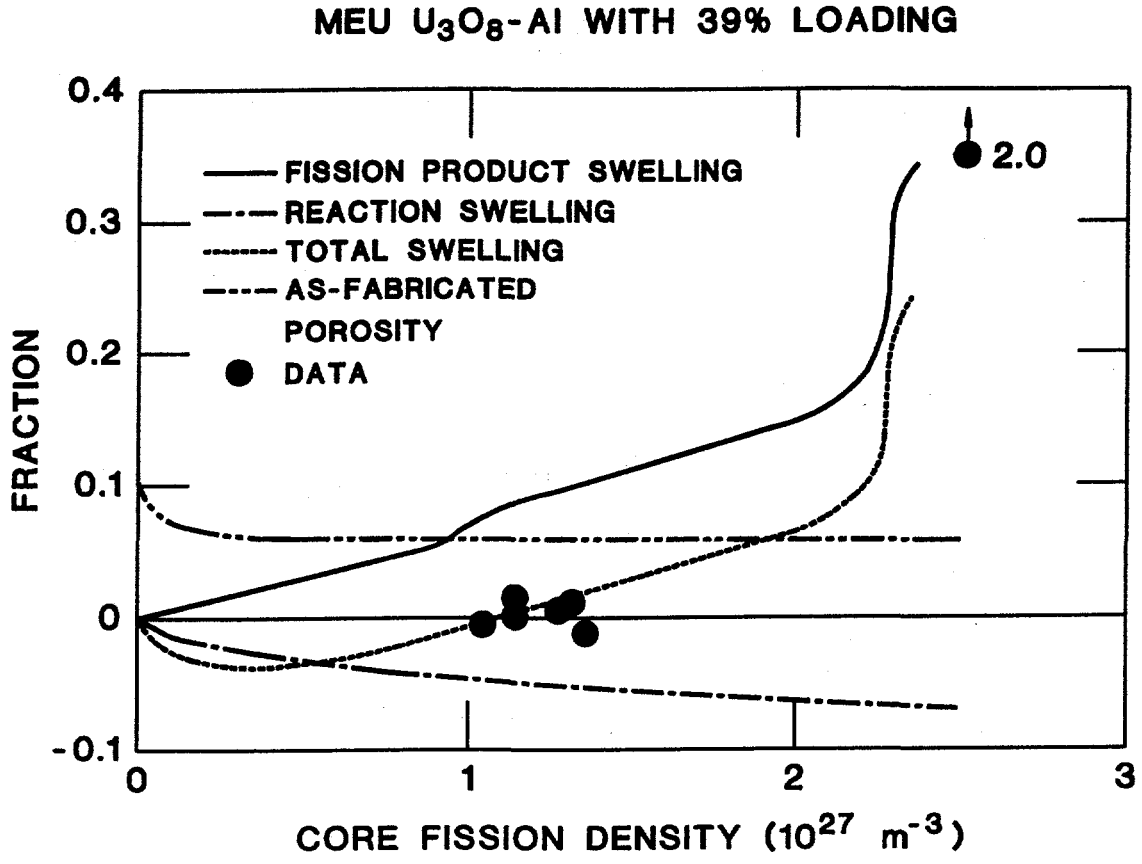

Fig. 11. DART Calculation for MEU U_3O_8-Al Plate with 39 vol.% Loading and LEU and MEU Miniplate Core Swelling Data

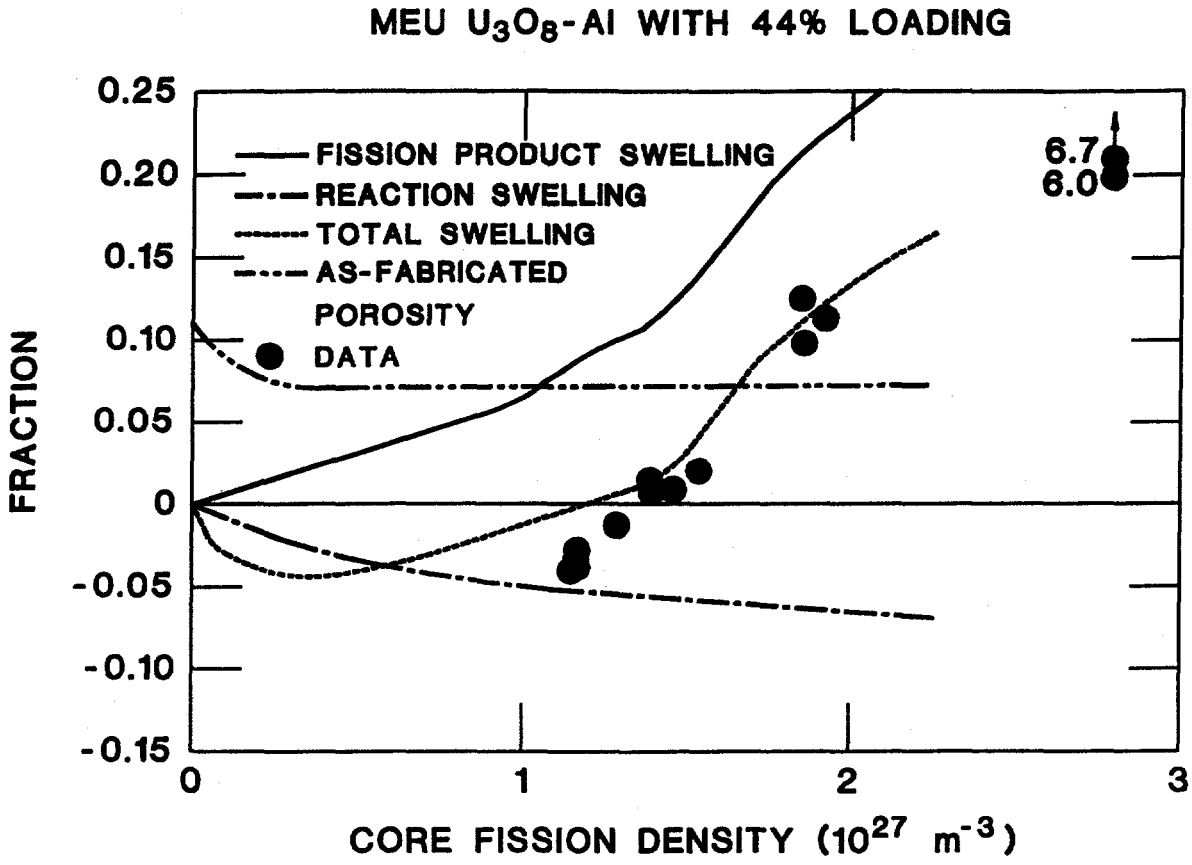

Fig. 12. DART Calculation for MEU U_3O_8-Al Plate with 44 vol.% Loading and LEU and MEU Miniplate Core Swelling Data

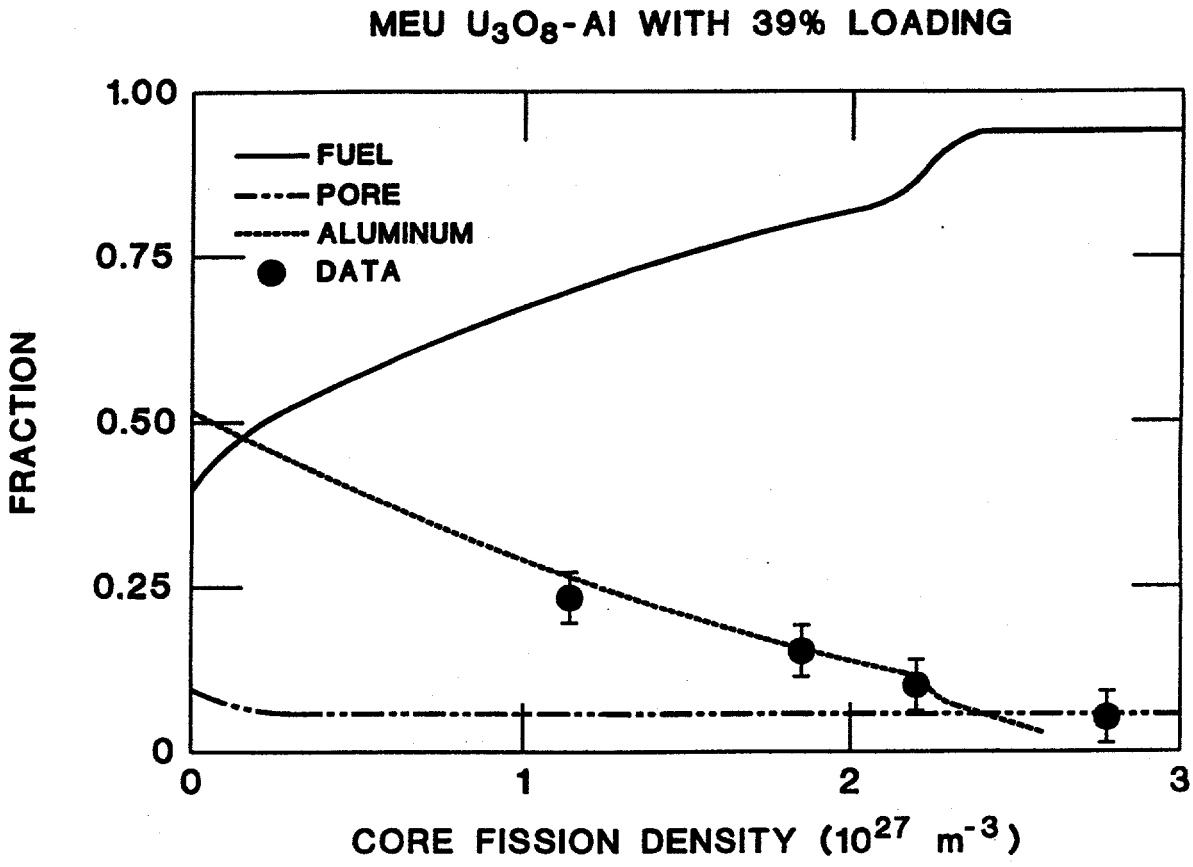

Fig.13. DART Calculation of Core Constituent Volume Fractions and Al Volume Fraction Data From Miniplates

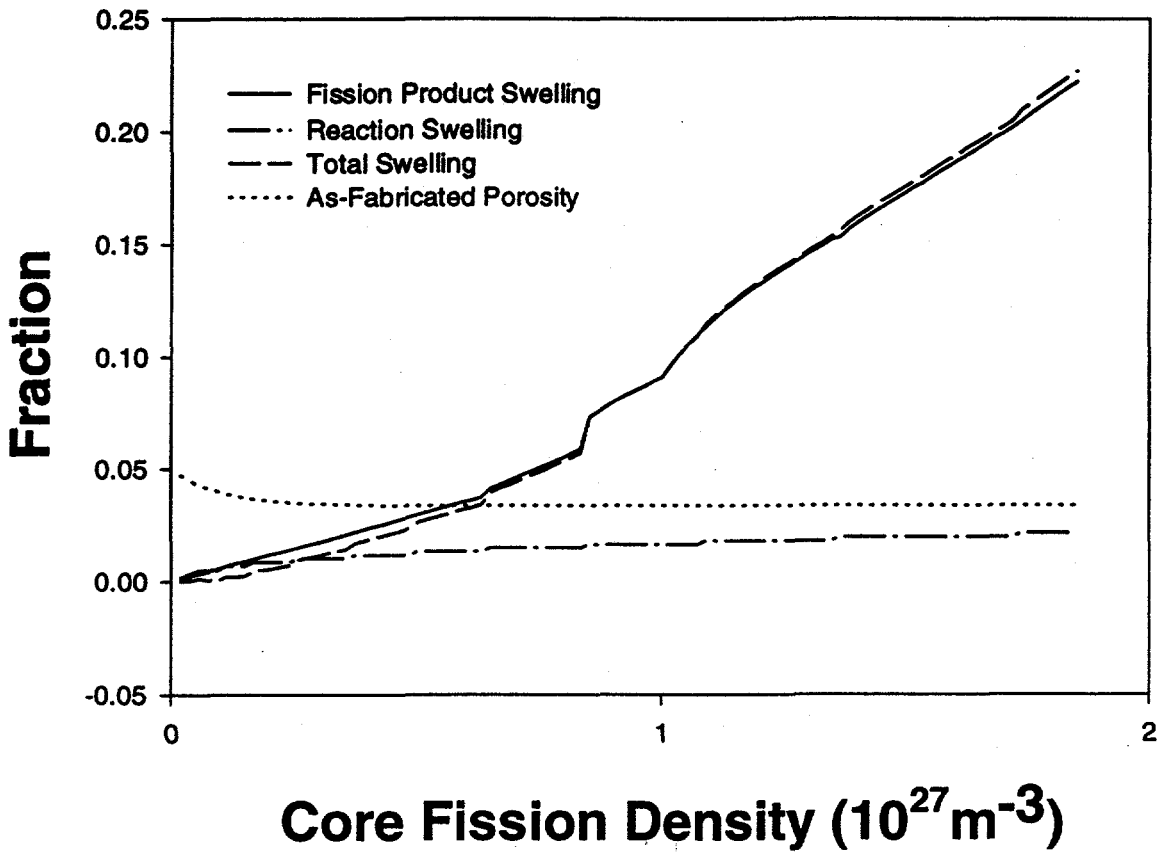

Fig. 14. DART Calculation for Tubular MR Element with 5 vol.% As-Fabricated Porosity and Irradiated at 100°C

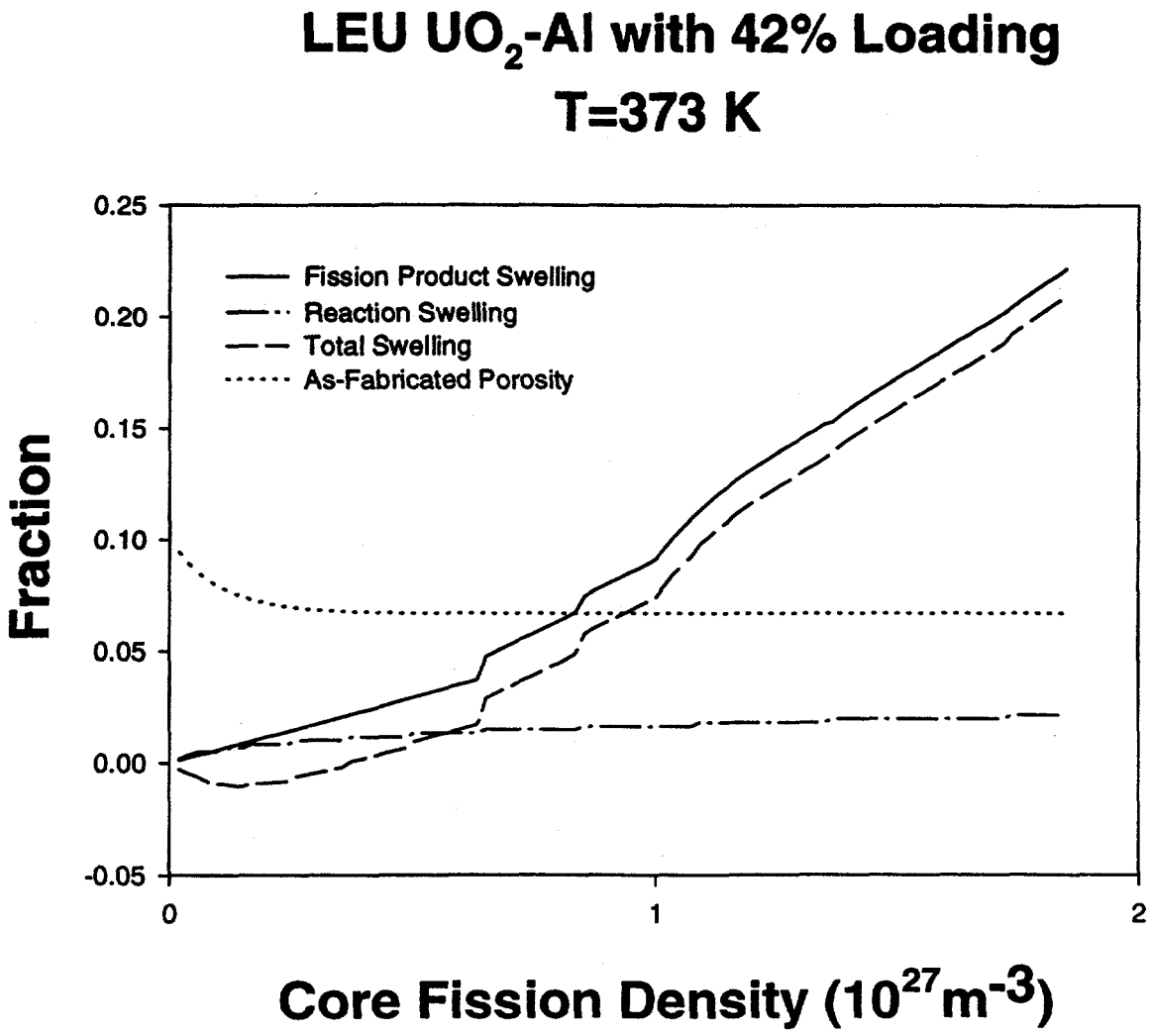

Fig. 15. DART Calculation for a Tubular MR Element with 10 vol.% As-Fabricated Porosity and Irradiated at 100°C

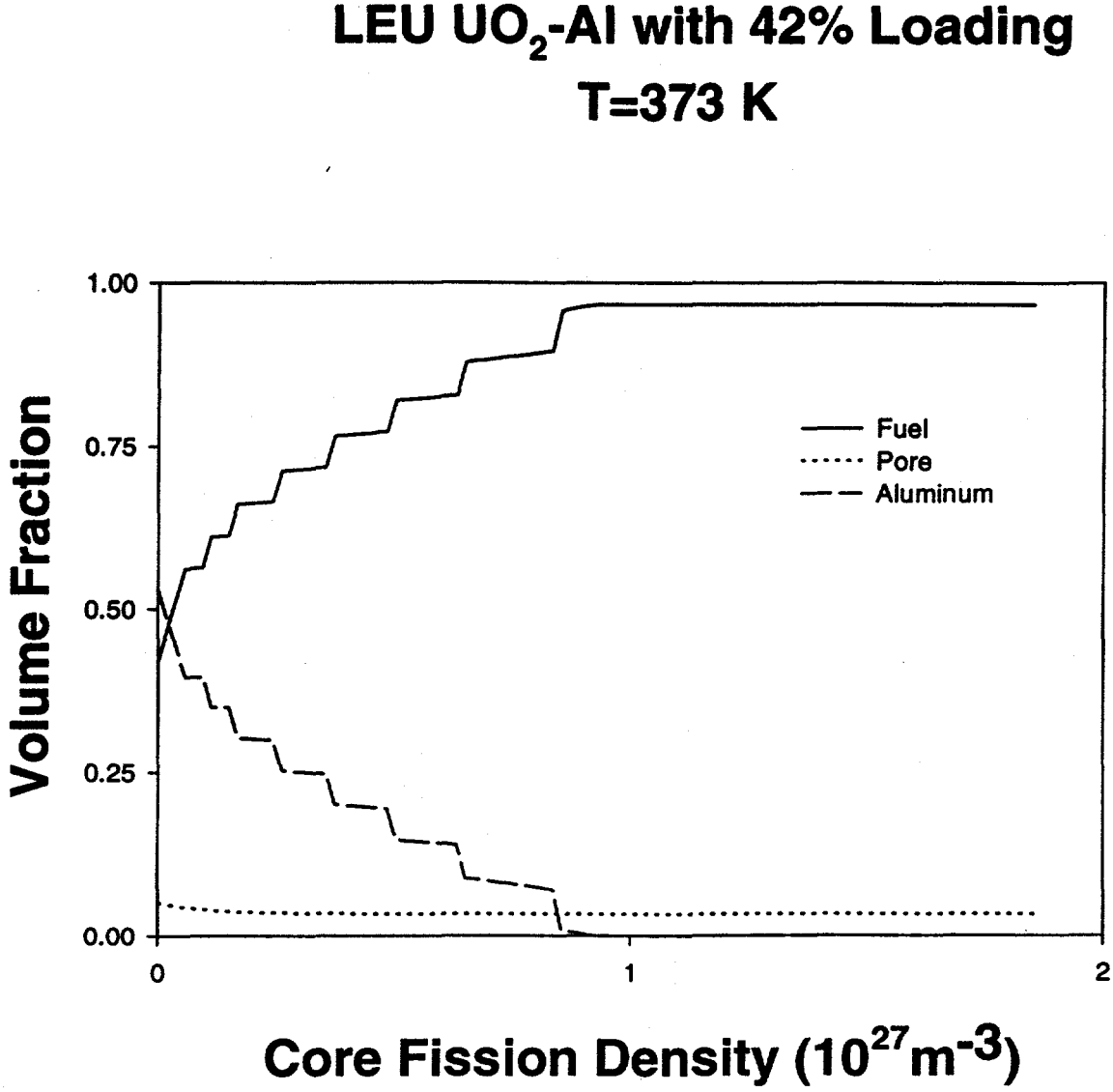

Fig. 16. DART Calculation of Core Constituent Fractions for a Tubular MP element with 5 vol.% As-Fabricated Porosity and Irradiated at 100°C

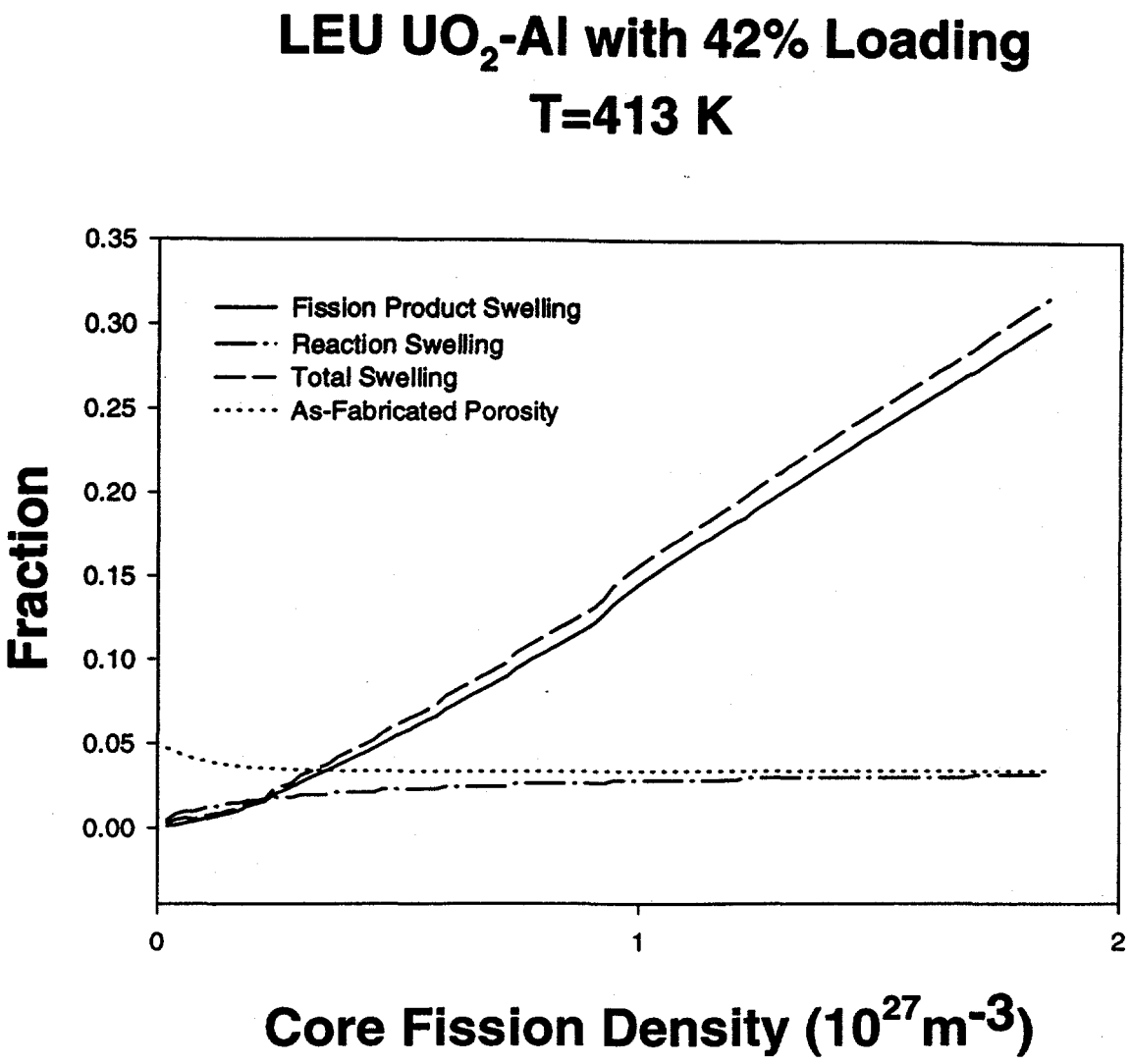

Fig. 17. DART Calculation for a Tubular MR Element with 5 vol.% As-Fabricated Porosity and Irradiated at 140°C

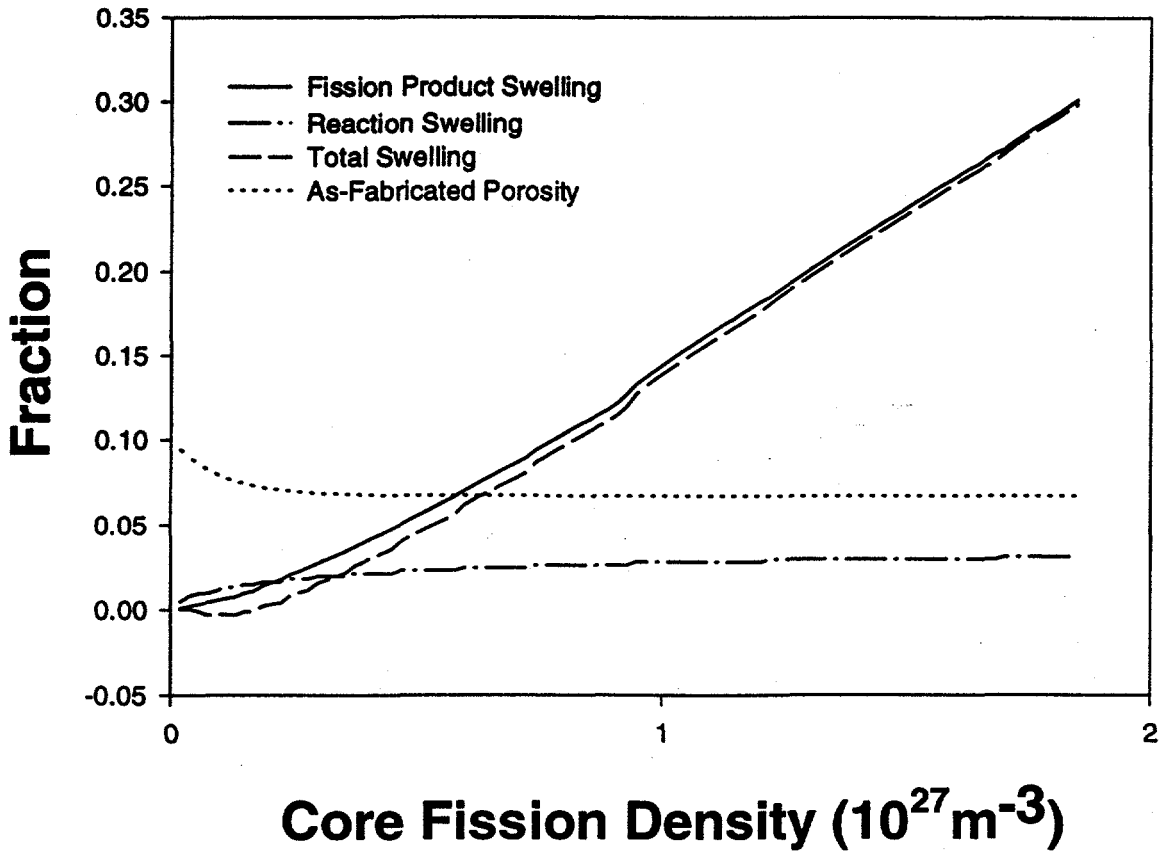

Fig. 18. DART Calculation for a Tubular MR Element with 10 vol.% As-Fabricated Porosity and Irradiated at 140°C

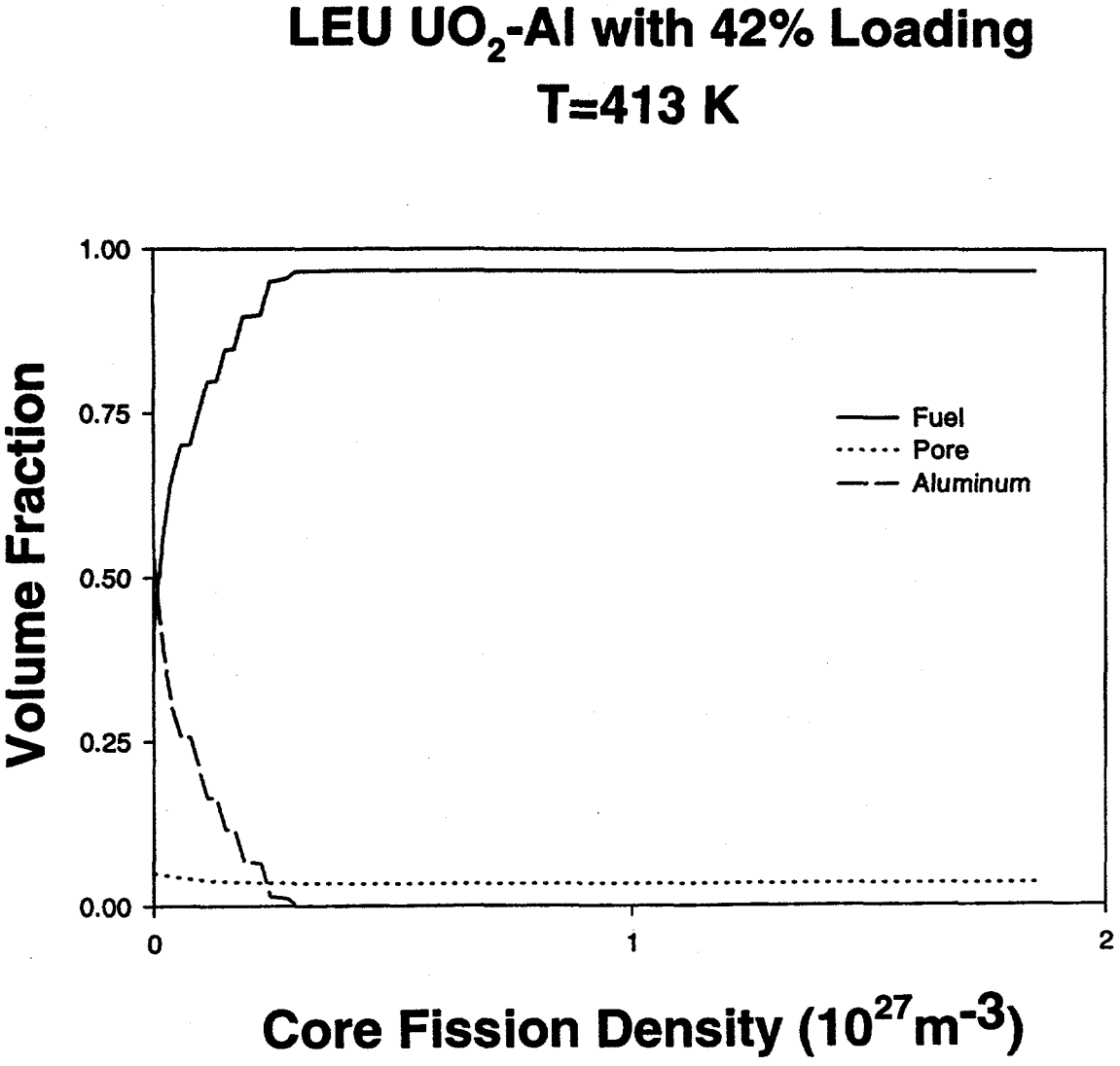

Fig. 19. DART Calculation of Core Constituent Fracions for an MP element with 5 vol.% As-Fabricated Porosity and Irradiated at 140°C

TABLE II
SWELLING DATA FOR U_3O_8-AL MINIPLATES

Plate No.	Wt.% U_3O_8	Original Volume Fraction			Core Fission Density ($X10^{21}$)	Swelling %
		U_3O_8	Al	Voids		
O-59-3	25.9	10.1	88.7	1.2	1.14	3.0
O-49-4	65.1	34.8	57.8	7.4	0.92	1.0
O-56-4	65.0	35.0	58.2	6.9	0.92	0.9
O-52-2	65.0	34.5	57.5	7.9	0.91	0.1
O-52-1	65.0	34.5	57.5	7.9	0.91	0.0
O-53-4	64.9	35.1	58.6	6.3	1.01	1.1
O-46-6	64.0	34.8	58.1	7.1	2.21	9.7
O-57-1	70.0	39.2	51.9	8.9	1.26	0.5
O-57-2	70.0	39.2	51.8	9.0	1.27	0.3
O-54-1	69.9	39.5	52.5	8.0	1.27	0.4
O-50-4	70.0	39.2	52.0	8.8	1.31	0.9
O-50-5	69.9	39.2	52.1	8.6	1.35	1.2
O-50-6	69.9	39.2	52.1	8.7	1.35	1.2
O-50-2	70.0	39.2	51.9	8.9	1.03	-0.7
O-57-4	70.0	39.4	52.1	8.6	1.04	-0.7
O-54-6	69.9	39.4	52.3	8.3	1.14	0.0
O-54-2	70.0	39.5	52.4	8.1	1.14	1.3
O-47-2	69.9	39.2	52.1	8.7	2.48	209.0*
O-51-1	74.9	43.9	45.4	10.7	1.16	-3.1
O-59-2	74.9	43.7	45.2	11.0	1.15	-3.8
O-51-5	75.0	44.0	45.4	10.5	1.16	-2.8
O-58-4	75.0	43.9	45.2	10.9	1.16	-3.8
O-58-6	75.0	43.9	45.2	10.9	1.16	-3.6
O-55-4	74.9	44.3	45.8	9.9	1.28	-1.3
O-55-3	75.0	44.2	45.4	10.4	1.28	-1.3
O-48-2	75.1	44.2	45.2	10.7	1.92	11.2
O-48-1	75.0	43.9	45.3	10.8	2.78	601.0*
O-48-6	74.9	43.9	45.4	10.7	2.78	670.0*
O-58-7	74.9	43.9	45.3	10.8	1.46	0.9
304N	61.8	32.6	62.2	5.2	1.37	2.1
308N	61.9	32.5	62.0	5.5	1.37	1.6
405N	63.8	34.0	59.5	6.5	2.00	2.9
407N	63.8	34.0	59.6	6.4	2.00	3.0
505N	74.6	43.5	45.8	10.7	1.39	0.9
506N	73.9	43.4	47.5	9.1	1.39	1.5
613N	75.0	44.3	45.7	10.0	1.86	9.8
614N	75.0	44.2	45.5	10.3	1.85	12.6
RA-209	64.7	35.0	58.9	6.2	1.22	1.7
RA-218	71.9	41.2	49.8	9.0	1.43	1.8
RA-219	64.9	34.8	58.2	7.0	1.21	1.8
RA-222	74.9	44.2	45.8	10.0	1.54	2.2

* Pillowed Plates
O-xx-x Oak Ridge National Lab
xxxN NUKEM
RA-xxx CNEA

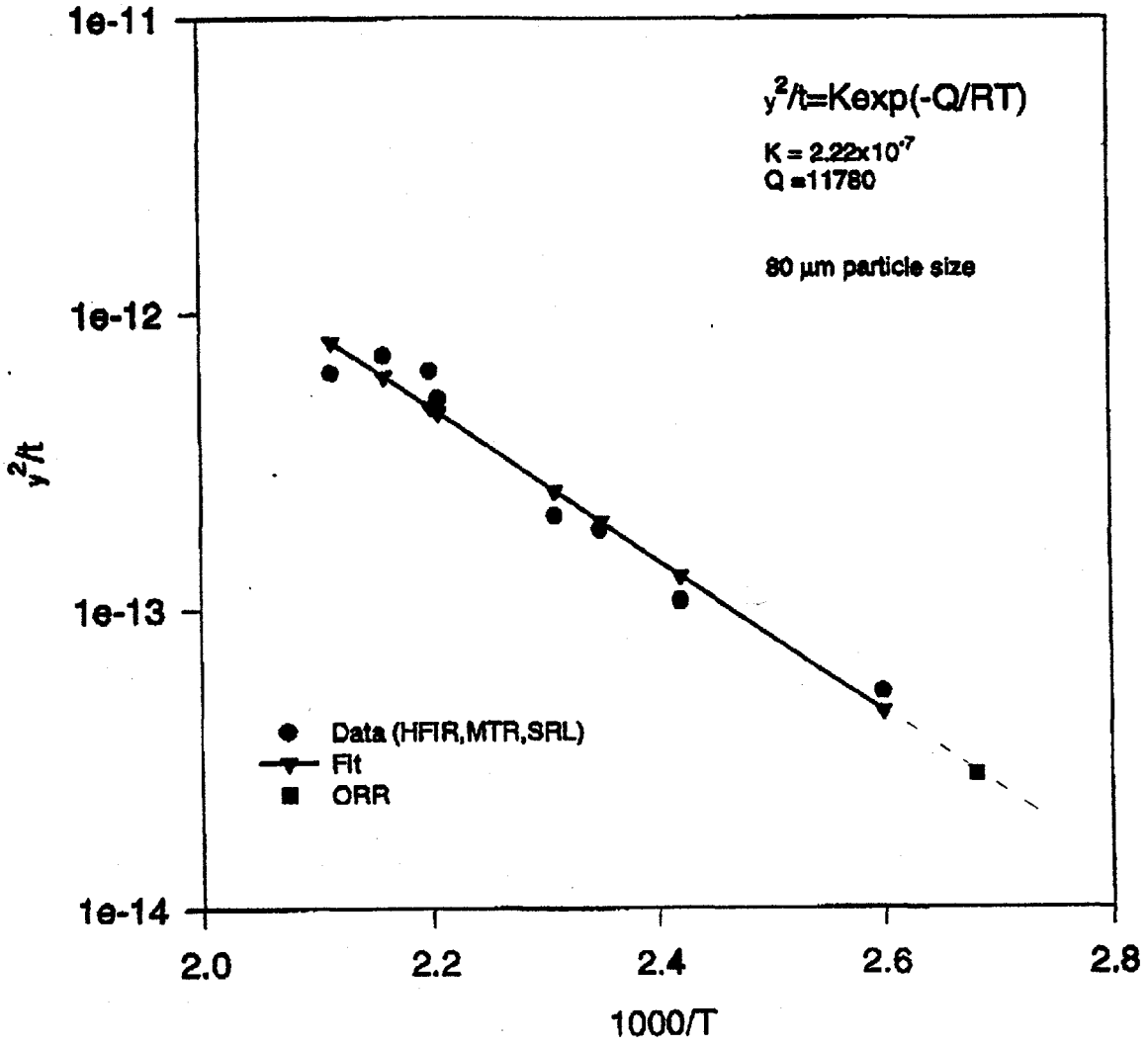
1e-11
1e-12
1e-13
1e-14
y^2/t
$y^2/t=Kexp(-Q/RT)$
K = 2.22x10^{-7}
Q =11780
80 µm particle size
Data (HFIR,MTR,SRL)
Fit
ORR
2.0
2.2
2.4
2.6
2.8
1000/T

Fig. 8.